#4886

Health Physics Vol. 59, No. 4 (October), pp. 405–419, 1990
Printed in the U.S.A.

0017-9078/90 $3.00 + .00

● *Paper*

DEVELOPING SOIL GAS AND ^{222}Rn ENTRY POTENTIALS FOR SUBSTRUCTURE SURFACES AND ASSESSING ^{222}Rn CONTROL DIAGNOSTIC TECHNIQUES

Bradley H. Turk,* Jed Harrison,† Richard J. Prill‡ and Richard G. Sextro
Indoor Environment Program, Applied Science Division, Lawrence Berkeley Laboratory, University of California, Berkeley, CA 94720

Abstract—**Research-based procedures for characterizing the causes of elevated indoor ^{222}Rn levels and guiding the selection of an appropriate control technique were evaluated at seven New Jersey houses. Procedures such as thorough visual inspections, blower door air leakage tests, pressure field mapping, subsurface vacuum extension tests, sampling of ^{222}Rn concentrations throughout the substructure, and measurements of the additional depressurization caused by various appliances all were found to furnish important information to the mitigation contractor or researcher. An analysis of data from these and other diagnostic techniques performed at the seven houses also indicated: (1) regions of very high permeability existed directly adjacent to the exterior of substructure walls and floors; (2) the additional substructure depressurization caused by operation of forced-air furnaces and attic exhaust fans could exceed 1 Pascal; (3) ^{222}Rn concentrations below basement slabs and slabs-on-grade adjoining below grade basement walls were approximately seven times higher than those within block wall cavities; and (4) air leakage areas of crawlspace and basement ceilings were quite large, ranging up to 0.15 m^2. The pressure field mapping tests identified the areas surrounding the substructure that were well coupled to the indoors. Using flow, pressure difference, and ^{222}Rn concentration data, indices of soil gas entry potential and ^{222}Rn entry potential were developed to indicate the areas of the substructure that may have high entry rates of soil gas and ^{222}Rn, respectively. These indices could be helpful for quantifying the relative resistance to soil gas movement of substructure surfaces and surrounding soils and for determining the placement of ^{222}Rn control systems.**

INTRODUCTION AND OVERVIEW

TO DEVELOP an effective and efficient system for long-term control of elevated ^{222}Rn in a building requires a thorough understanding of the interaction of the building and its systems with the movement of ^{222}Rn in the soil. To assist researchers and private-commercial contractors, a number of procedures and diagnostic measurement techniques have been developed to improve our knowledge of ^{222}Rn entry and of practical ^{222}Rn control methods (Brennan 1988; Harrje et al. 1987; Gadsby et al. 1989; Sanchez et al. 1987; Turk et al. 1987a). Radon-222 control diagnostic techniques are a set of tests and procedures that are systematically applied to a structure with elevated indoor ^{222}Rn levels for the purposes of: (1) identifying the source(s) of ^{222}Rn; (2) understanding the mechanisms by which ^{222}Rn interacts with and enters the building; and (3) selecting, designing, and installing an appropriate control technique that will effectively and economically reduce long-term ^{222}Rn levels below accepted guidelines under changing conditions of environment and occupancy.

The research described in this paper is the continuation of an exploratory study of the utility of various diagnostic techniques, done as part of an intensive examination of Rn entry and control in seven New Jersey homes. This preliminary work has been previously reported in Turk et al. (1987a). An initial evaluation of diagnostic techniques was also conducted as part of a study of Rn mitigation in 15 houses in the Pacific Northwest (Turk et al. 1987b). An objective of the research discussed here was to develop and evaluate diagnostic techniques to assist in the design, installation, and operation of appropriate ^{222}Rn control systems. Another practical goal was to reduce the winter indoor ^{222}Rn levels in these houses to below that of the U.S. Environmental Protection Agency (EPA) 1986 action level guideline for annual concentrations of 148 Bq m^{-3}(4 pCi L^{-1}). Because they are part of a research effort, some of the techniques described here may have broader application to the study

(*Manuscript received* 23 *June* 1989; *revised manuscript received* 11 *April* 1990, *accepted* 30 *May* 1990)

* Current address: Room 109, 105 E. Marcy Street, Santa Fe, NM 87501.

† Current address: Office of Radiation Programs, U.S. Environmental Protection Agency, 401 M Street SW, Washington, D.C. 20460.

‡ Current address: Washington State Energy Extension Service, N. 1212 Washington, Spokane, WA 99201.

of soil gas (and ^{222}Rn) transport. Others, in their present form, may be of limited practical use to contractors.

DESCRIPTION OF PROCEDURES

The general sequence of events leading to the installation of a ^{222}Rn control system in a house can be briefly described, as follows. Diagnostic procedures are initiated after elevated indoor ^{222}Rn levels have been confirmed. While the pressure-driven flow of soil gas (containing ^{222}Rn) into buildings is the primary cause of elevated indoor ^{222}Rn levels in the vast majority of structures, an inspection of the building can suggest whether possible non-soil sources (domestic water and building materials) should be tested. The structure and entry points are further characterized through various tests and measurements. An appropriate mitigation system or technique is then designed and installed, followed by short-term measurements of indoor ^{222}Rn levels and system operating parameters. If necessary, the mitigation system is modified to improve its effectiveness in reducing indoor ^{222}Rn concentrations, again verified by short-term measurements, and by long-term follow-up monitoring of indoor ^{222}Rn levels.

While other mitigation techniques may be necessary in certain situations, subsurface ventilation (SSV) through depressurization (SSD) or pressurization (SSP) of the soil and materials adjacent to the exterior of below-grade floors and walls is successful in most houses. Consequently, many of the diagnostic tests are directed toward the design and implementation of these types of systems. Brief descriptions of the prospective diagnostic techniques are provided in the following paragraphs. More complete descriptions of these diagnostic techniques, the criteria used for selection of the mitigation systems, and descriptions of the systems and their performance are provided in Turk et al. (1987a, 1988).

Visual inspection

The visual inspection consisted of a complete tour of the building with the owner/occupant and building plans, if available. In addition, standardized forms (Turk et al. 1987a) were completed that requested pertinent information on construction characteristics, substructure holes and imperfections that open to the soil, mechanical system operation, and occupant effects (window openings, appliance operation, occupancy times and locations, etc.). A floor plan was sketched and dimensioned. Photographs were sometimes helpful, including any that were taken during construction of the substructure.

If the water supply was from a private well or the municipal supply was known to have elevated levels of ^{222}Rn (more than $\sim 1.5 \times 10^6$ Bq m^{-3}), it was noted that the water was a possible significant source of indoor ^{222}Rn. Likewise, it was also noted if the house had large quantities of exposed earth-based construction materials (e.g., brick, adobe, stone, etc.) that might be suspected of containing significant radionuclide mineralization.

Building material surface ^{222}Rn flux

A metal pan (21.6-cm diameter), containing two charcoal adsorption canisters, was sealed with a non-drying putty or caulk to the surfaces of building materials suspected of having high ^{222}Rn emanation rates (walls, floors, etc.) caused by excess ^{226}Rn in the material. After exposure for 24 to 48 h, the canisters were analyzed by γ spectrometry and the ^{222}Rn flux density from the surfaces was calculated. Based on variations in exhalation rates and errors in exposure time, analytical technique, and sampling technique, the uncertainty in the calculated ^{222}Rn flux was estimated at ±20%. Because these measurements were made *in situ,* a component of the flux is due to diffusion of ^{222}Rn from the surrounding soil. However, for the purposes of rating the importance of the various ^{222}Rn entry mechanisms in a particular house, a measurement that combines diffusive transport of ^{222}Rn from the soil and from the construction materials is appropriate. The contribution to indoor air ^{222}Rn concentrations was estimated from the ^{222}Rn flux normalized by indoor volume:

$$F_v = (FA)/V, \quad (1)$$

where F_v = volume-normalized source rate (Bq m^{-3} s^{-1}), F = flux density (Bq m^{-2} s^{-1}), A = material surface area (m^2), and V = building/zone volume (m^3).

If a ventilation rate of 0.5 air changes per hour (ach) is assumed for a building, then a value of F_v greater than 0.021 Bq m^{-3} s^{-1} may indicate that ^{222}Rn from building materials could contribute more than 148 Bq m^{-3} to the indoor air.

Radon-222-in-water concentrations

Research suggests that ^{222}Rn concentrations in the domestic water supply will result in ^{222}Rn concentrations in indoor air that are approximately 10,000 times lower than those in the water (Gesell and Prichard 1980; Nazaroff et al. 1985). For the study reported in this paper, two methods were used to determine the ^{222}Rn concentrations in the domestic water supplies. The direct method involved collecting samples of water in 1-L polyethylene bottles from faucets where the water was not filtered or aerated. The ^{222}Rn activity in the bottles was then analyzed by γ spectrometry. Samples were collected twice: in the late fall of 1986 and in August of 1987. The estimated uncertainty for collection and analysis was 10%. Concentrations of ^{222}Rn in water greater than 1.5×10^6 Bq m^{-3} indicated that the water may be an important source of indoor ^{222}Rn.

An alternative technique was performed from two to four times at each house. A bathroom shower was operated for 10 to 15 min with the bathroom door closed and ventilation systems off. Grab samples of bathroom air were collected before and after the shower was operated. The ^{222}Rn concentrations [$C(t)$ and $C(o)$, respectively, in Bq m^{-3}] along with the elapsed time, t (h); room volume, V (m^3); shower flow rate, W (m^3 h^{-1});

and a transfer coefficient, E, of 0.9 were used to estimate concentrations of ^{222}Rn in water, C_w (Bq m^{-3}), from:

$$C_w = \frac{V[C(t) - C(o)]}{EWt}. \quad (2)$$

Appliance effects

The operation of many devices often found in residences (exhaust fans, clothes dryers, combustion devices, and forced air furnaces) can cause additional depressurization of substructures (Mowris and Fisk 1987). These devices were cycled on and off up to 20 times while substructure-outside pressure differences were monitored. The change in the average pressure difference when the device is cycled between "on" and "off" is the additional depressurization (or pressurization) experienced by the substructure during appliance operation.

Soil air permeability

Air permeability of soil was measured *in situ* using techniques described in DSMA (1983) and Turk et al. (1987b). To map the vertical and horizontal variations in soil characteristics, these measurements were made at approximately 25 locations in the soil outside each house at depths ranging from 0.3 to 2.2 m and distances from the houses ranging from 0.5 to 3.5 m. The probe at each of these locations was a capped galvanized pipe (13 mm outside diameter). The data may help to identify regions of soil where soil gas bearing ^{222}Rn is more readily transported to the substructure.

In each house, approximately 30 test holes (6 mm to 13 mm in diameter) were drilled through substructure slab floors and hollow block walls and into the block cavities of these walls (approximately 0.25 m above the floor) for a variety of measurement purposes. Permeability was measured at a distance of 0.01 to 0.02 m from the exterior of the structure through several of the test holes. A few measurement locations extended approximately 1 m below the slab floors. These data describe the approximate permeability of near-house materials and may indicate the presence of gaps and channels between the building and these materials.

Blower door tests

Depressurization by a blower door was used to determine the effective air leakage area (ELA) of each house and of the zones (superstructure, substructure) within each house (ASTM 1981). The ELA for the whole house was measured with the door connecting the superstructure to the substructure open. The ELA for the superstructure was measured with the door closed but with the substructure windows and vents open. The substructure ELA was measured by placing the blower door at the door to the substructure and with the superstructure doors and windows open. ELAs for the substructure ceiling and substructure walls and floors were then calculated from Turk et al. (1987a):

$$\mathrm{ELA}_c = (\mathrm{ELA}_p + \mathrm{ELA}_b - \mathrm{ELA}_w)/2, \quad (3)$$

and

$$\mathrm{ELA}_f = \mathrm{ELA}_b - \mathrm{ELA}_c, \quad (4)$$

where ELA_w = whole building ELA, ELA_p = superstructure ELA, ELA_b = substructure ELA, ELA_c = substructure ceiling ELA, and ELA_f = substructure basement walls and floor ELA.

The flow-calibrated blower door was also used to pressurize basements to determine the flows necessary to achieve successful ^{222}Rn control by basement overpressurization of a few Pascals. A power curve was fitted to the blower door data so that flows could be calculated at pressure differences other than those used in the test.

Grab samples of ^{222}Rn

To identify areas of high ^{222}Rn gas concentration, samples of air were collected from outdoor soil probes, indoor test holes, and suspected entry points using a hand pump and evacuated α-scintillation cells. The activity in the cells was then measured with a portable photomultiplier-tube counting station. Indoor samples were collected under both natural environmental conditions and during a 10-Pa depressurization of the substructure that was imposed by the blower door. Errors in ^{222}Rn concentrations measured with this procedure were approximately ±20%.

Subsurface air flow and vacuum field extension

A single-speed industrial vacuum pulled air through a test hole in the slab floors and depressurized the subslab space to simulate a subsurface depressurization mitigation system. During vacuum operation, pressure differences (referenced to the basement with the test holes sealed) and air velocities (with the test holes open) were measured at the other test holes throughout the basement to determine the extent and spatial distribution of the pressure field. Those test holes with the largest pressure differences and flow rates were better connected to the vacuum hole (i.e., the resistance to flow between the vacuum and test holes is less); thus, an SSD mitigation system would be more likely to control soil gas and Rn entry near these test holes.

Pressure field mapping

The substructure of each building was depressurized with a blower door to approximately −30 Pa, while pressure differences, referenced to the basement, were measured at the outdoor soil probe locations and at several of the indoor test holes (Nazaroff et al. 1986). Additional tests were conducted at approximately −30 Pa and −10 Pa in some of the houses. In these later tests, more of the indoor test hole locations were surveyed. Air velocities at the open test holes were measured, and pressure differences across the test holes were measured with the test holes sealed. These data were used in the development of

entry potentials for soil gas and Rn. Ratios of the pressure differences at the test holes or soil probes to the basement depressurization relative to outside (coupling ratios) provide a measure of the extension of the pressure fields from the house. Smaller ratios may result from nearby cracks and openings in the substructure surfaces or from more distant openings that are connected via high permeability pathways to the test holes, and therefore indicate good coupling with the interior of the substructure. Air velocities as small as approximately 0.025 m s^{-1} were measured with a hot wire anemometer attached to a flow adaptor designed to mate with the test holes (Fig. 1). At velocities of 0.7 m s^{-1}, the pressure drop across the flow adaptor was estimated to be approximately 0.5 Pa. Small quantities of chemical smoke were directed at the surface of the test holes to provide qualitative information on the relative velocity and direction of the air moving through the test holes.

DATA PRESENTATION

Examples of data are shown on a site plan for house LBL14C in Figs. 2 and 3. Table 1 is a key for the symbols used in the drawings. Similar data for the remaining six houses and other data from diagnostic measurements in all houses are presented in the appendices of Turk et al. (1989b).

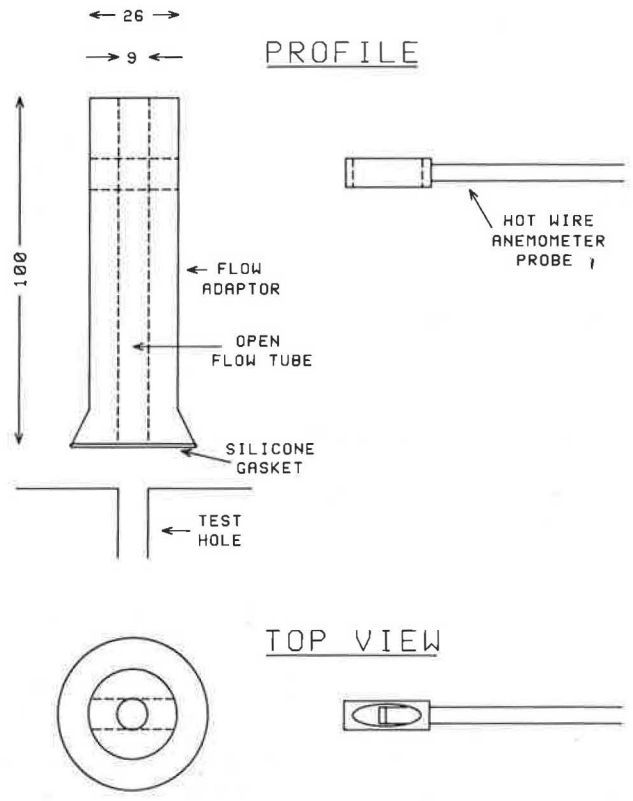

Fig. 1. Flow adaptor device used to measure flows through test holes during various tests. The bottom opening of the adaptor seals against the test hole surface, while flows are measured with a hot wire anemometer probe placed inside the open tube of the adaptor. Dimensions are in millimeters.

Table 1. Key to symbols for Figs. 2 and 3.

Locations
- *I* = Indoor
  - *W* = Wall
    - (*B*) = Into block wall cavities
    - Blank = Through wall into soil
    - Top = Opening at top of wall
  - *F* = Through floor
- *O* = Outdoor
  - A = ~0.5 m from house
  - B = ~1.5 m from house
  - C = ~3.0 m from house
  - N, E, W, S = Orientation to compass direction
- 1, 2, 3, · · · = Arbitrary sample location number
- SSD Pipe = Subsurface depressurization pipe for radon control system
- Vac. Hole = Test hole where vacuum was placed for pressure field extension tests

Measurements
- PFM = Pressure field map coupling ratio ($\Delta P_{TESTHOLE}$) ($P_{OUTSIDE} - P_{BASEMENT}$)$^{-1}$
  - I = Initial test, basement depressurized to −30 Pa
  - 10 = Basement depressurized to −10 Pa
  - 30 = Basement depressurized to −30 Pa
  - OR = Over range
- *K* = Permeability (10^{-12} m^2)
- *R* = ^{222}Rn concentration (1000 Bq m^{-3})
  - (Dates) S = Sep 86
    - O = Oct 86
    - M1 = First May 87 test
    - M2 = Second May 87 test
    - J1 = First June 87 test
    - J2 = Second June 87 test
    - J3 = Third June 87 test
    - D = Diagnostic test
- *V* = Vacuum test ratio ($\Delta P_{TESTHOLE}/\Delta P_{VACUUMHOLE}$) × 10^{-3}
- *G* = Soil gas entry potential (10^{-6} m^3 Pa^{-1} s^{-1})
- *E* = ^{222}Rn entry potential (10^{-3} Bq Pa^{-1} s^{-1})

Building material surface ^{222}Rn *flux*

The emanation of ^{222}Rn from the surfaces of building materials varied by more than three orders of magnitude. A flux density of 0.0009 Bq m^{-2} s^{-1} was measured at one floor (LBL09) and one block wall (LBL14) location, 0.47 Bq m^{-2} s^{-1} at one block wall location (LBL10), and 1.9 Bq m^{-2} s^{-1} on another block wall (LBL10). The high flux densities measured on the block wall surfaces may indicate that ^{222}Rn in the soil gas adjacent to the exterior of the walls is rapidly diffusing through the porous block materials or that the measurement pan was poorly sealed to the irregular surface of the block. For all houses tested, the arithmetic mean flux density from 10 measurements on concrete slab floors was 0.013 Bq m^{-2} s^{-1} [geometric mean (GM) of 0.0085 Bq m^{-2} s^{-1}, geometric standard deviation (GSD) of 3.2] and the arithmetic mean flux density from 13 measurements on block walls was 0.24 Bq m^{-2} s^{-1} (GM of 0.033 Bq m^{-2} s^{-1}, GSD of 9.9). If the one extremely high flux density from a block wall surface is eliminated, the arithmetic mean for walls becomes 0.10 Bq m^{-2} s^{-1} (GM of 0.024 Bq m^{-2} s^{-1}, GSD

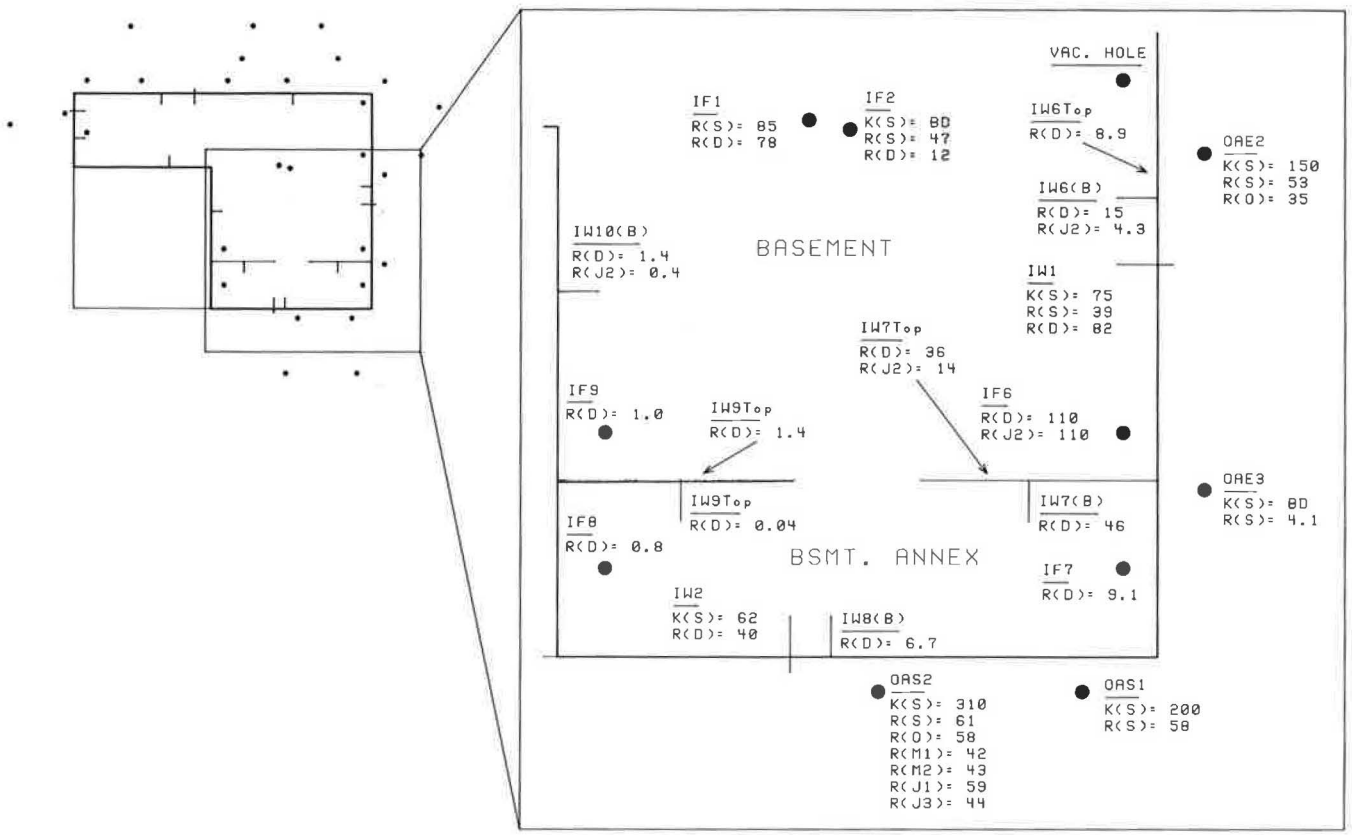

Fig. 2. A site plan of house LBL14C showing the locations of probes in the soil around the house, holes drilled through the slab floors (solid dots), and test holes drilled into and through hollow block walls (vertical and horizontal lines). Measured data for soil air permeabilities (K) and ^{222}Rn grab samples (R) are mapped with the identification of the test hole. Measurements for a section of the basement are shown in an exploded view on the right. (See Table 1 for more complete descriptions of the codes used.)

of 7.6). These data can be compared with the range of 0.0009 Bq m^{-2} s^{-1} to 0.0067 Bq m^{-2} s^{-1} for earth-based construction materials presented in Nero and Nazaroff (1984).

Corresponding ^{222}Rn entry rates were calculated by multiplying the flux density by the appropriate surface area (m^2). The building volume-normalized source rate (F_v) was then estimated for each house. Only the source rate of 0.074 Bq m^{-3} s^{-1} at LBL10 using the suspect high flux data exceeded the target of 0.021 Bq m^{-3} s^{-1}. There was no other information to suggest that the block walls in this house contained Ra-rich materials.

Radon-222-in-water concentrations

Direct γ spectrometric analysis of ^{222}Rn concentrations in water showed a range of 4100 Bq m^{-3} (at LBL13) to 310,000 Bq m^{-3} (at LBL08 with a private well). Differences between the two seasonal samples (collected at six houses) were quite large, ranging from 31,000 to 39,000 Bq m^{-3} at LBL12, 135,000 to 310,000 Bq m^{-3} at LBL08, and 8100 to 46,000 Bq m^{-3} at LBL10. None of these ^{222}Rn-in-water concentrations is expected to contribute more than approximately 30 Bq m^{-3} to the indoor air concentrations.

The alternate method of measuring bathroom air concentrations before and after shower operation yielded disappointing results. Equivalent water concentrations calculated from this method usually did not replicate, were occasionally negative, and were not consistently within the range of concentrations measured by the direct method. This technique was unsuccessful for several reasons. First, in some houses, low concentrations in bathroom air were difficult to measure accurately because of residual background activity in the α-scintillation cells used to collect the grab samples. Second, in some houses, other stronger ^{222}Rn sources elevated bathroom air concentrations so that the contribution from the water supplies with low concentrations was overwhelmed. Thus, the calculation involved subtracting one large and uncertain number from another.

Depressurization by appliances

The range of additional depressurization in substructure spaces due to the operation of various appliances

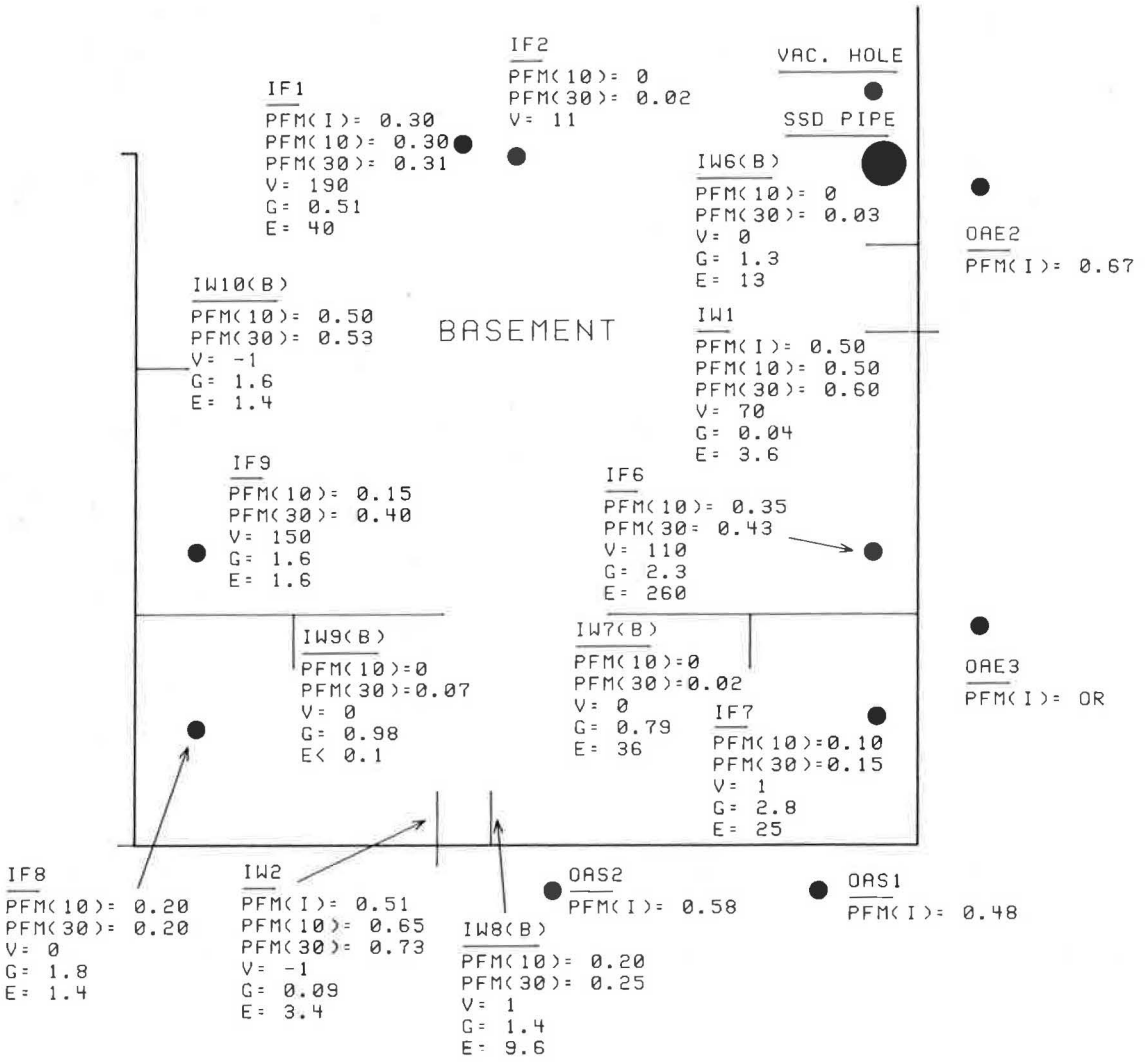

Fig. 3. Another exploded view of the same basement section in Fig. 2, except that data for coupling ratios during pressure field mapping tests (PFM), vacuum field extension tests (V), soil gas entry potentials (G), and ^{222}Rn entry potentials (E) are mapped. The single SSD pipe penetrated the slab along the east wall. The pressure difference at the vacuum hole location during testing was −770 Pa. (See Table 1 for more complete descriptions of the codes used.)

in the houses was difficult to quantify because the pressure differences were small and variable. The variation was usually caused by wind and the opening of windows, duct registers, and interior doors. In the five houses where pressure differences were monitored as only furnace burners were cycled on/off, the additional depressurization was always less than the 1 Pa detection limit of the portable electronic micromanometer (Table 2). By contrast, in five of the six homes with a forced-air furnace, the blower caused measurable (>1 Pa) additional depressurization. Air leaks in return plenums and ducts located in the substructure, along with substructure supply and superstructure return vents closed by the occupants, created this effect.

Although electric fans that exhaust hot air from the attic usually operate only in the summer, they had a surprisingly large impact, lowering basement pressures by almost 17 Pa in house LBL08. The negative pressure developed by the fans is communicated via bypasses (e.g., flue and chimney chases) that connect the attic to the basement. The effect of a whole house fan in one house was minimal, reducing basement pressure by approximately 1 Pa, since windows were usually open during operation of the fan. Clothes dryers (that exhaust to the outside) lowered basement pressures by 2 Pa or less.

It has been shown that 40 to 90% of the air exhausted by an SSD system may originate in the basement (Turk et al. 1989a). By assuming withdrawal rates of 0.0094 m^3 s^{-1} (20 cfm) and 0.0353 m^3 s^{-1} (75 cfm), the amount of additional basement depressurization due to operation of SSD systems, which simply adds to the depressurization from other mechanisms (Mowris and Fisk 1987), was

Table 2. Additional basement depressurization due to appliance operation.

Additional basement depressurization [a] (Pa)	Number of houses					
	Furnace burner only	Furnace blower only	Furnace burner + fan	Clothes dryer	Whole house fan	Attic fan
< 1	5	0	1	1	0	0
1 to < 2	0	2	1	1	1	0
2 to < 4	0	1	1	1	0	1
4 to < 6	0	0	1	0	0	1
6 and greater	0	1	0	0	0	1
Total number	5	4	4	3	1	3

[a] Ranges of additional depressurization include the ranges observed to occur at each house. For example, various duct register openings at LBL12 caused the additional depressurization to range from <1 to 1.5 Pa.

calculated for each house using the substructure ELA_b. Only the higher withdrawal rate in houses with tight substructures (LBL11 and LBL12) would cause a significant additional depressurization (−0.5 Pa and −0.2 Pa, respectively).

Soil air permeability

Examples of data from the permeability (K) measurements from LBL14C are summarized in Fig. 2. If multiple pressures were used, the permeability at the lowest pressure is presented. The data from all houses ranged from below the minimum detection limit ($\sim 1 \times 10^{-14}$ m^2) to near the maximum detection limit ($\sim 1 \times 10^{-8}$ m^2). The measurement values often replicated within a factor of 2, with the differences attributed to the precision of the measurement system and to changes in soil moisture between measurements. We have aggregated the measurements from the seven homes in order to illustrate the broad differences in the permeabilities of the various regions adjacent to the substructure. Because the data exhibit such a large range, as indicated by the large GSDs, only qualitative comparisons can be made.

The geometric mean of permeabilities for the soil probes surrounding the houses was approximately 40×10^{-12} m^2, with a geometric standard deviation of 22.1 (Turk et al. 1989a). Permeability measured in the ring of probes placed approximately 0.5 m from the house may be higher due to the less tightly packed backfill material (Sextro et al. 1989). The permeability of the gravel layer below slabs was quite high (GM of 890×10^{-12} m^2 with a GSD of 16), with individual values approaching the maximum detection limit. By contrast, permeability values from probes that penetrate into the compacted soil below the subslab gravel layer were much lower (GM of 0.16×10^{-12} m^2 with a GSD of 57). The permeability within 0.01 to 0.02 m of the exterior surfaces of walls was often very high, with a GM of 610×10^{-12} m^2 and a GSD of 8.4.

Blower door tests

Measured and calculated effective leakage areas are summarized in Table 3. Whole house ELA_ws varied from house to house by a factor of approximately 3, but the substructure ceiling (ELA_c) and substructure wall/floor (ELA_f) leakage areas varied by a factor of approximately 9. The whole house ELA_w was always smaller than the sum of the substructure and superstructure leakage areas because the latter two each included the leakage of the substructure ceiling, which can be large. In LBL14C, which had the tightest overall building shell, the substructure ceiling had almost twice the leakage of the overall structure. The large leakage area of substructure ceilings can be attributed primarily to holes and openings in the ducts of forced-air furnaces, but also to combustion appliance flues and to service penetrations and bypasses to attics. Since the forced-air furnaces were located in the basements of these houses, the return air and fan blower plenum also added significant leakage area. It is instructive to note the low substructure ceiling ELA for house LBL11, which had a hydronic heating system and therefore no ducts for air distribution.

The results of two blower pressurization tests performed on the basement of LBL11 were used to predict the flow rates necessary to overpressurize the basement for ^{222}Rn control. These predicted flows are compared with flows measured with the overpressurization system in operation at three different pressures, as illustrated in Table 4. The existing natural depressurization plus the system-induced overpressurization give the total pressure difference (ΔP) that was developed by the basement pressurization fan. As can be seen in Table 4, the predicted flows vary, which may be due to inaccuracies in measuring the small pressure differences during the blower door test and system operation and in the power curve fitting procedures applied to these data points. Although such predictions may not be used for determining the exact fan size required, the results do provide a general idea of the feasibility of pressurizing the basement.

Table 3. Effective air leakage areas (ELA).

House ID	Effective leakage area [m^2 (no. of measurements)] Whole house (ELA_w)	Substructure (ELA_b)	Superstructure (ELA_p)	Substructure ceiling (ELA_c)	Substructure walls + floor (ELA_f)
8	0.17	0.28	0.19	0.15	0.13
9	0.14(3)	0.13(3)	0.13(3)	0.061	0.073
10	0.14(2)	0.16	0.22	0.12	0.043
11[a]	0.087(2)	0.041	0.081	0.018	0.024
12[a]	0.078	0.068	0.12	0.053	0.015
13	0.12	0.14	0.20	0.11	0.026
14	0.06	0.13	0.14	0.10	0.023

[a] After air-leak tightening of basement for installation of basement pressurization Rn control system.

Note: Unless otherwise indicated, only one measurement was used.

For the first and last measurement dates indicated, the average measured pressure differences across the substructure ceiling were 7.1 Pa and 8.3 Pa, respectively. Using these pressure differences and an ELA_c of 0.018 m^2, flow rates from the basement to first floor were calculated to be 0.058 $m^3\ s^{-1}$ (120 cfm) and 0.130 $m^3\ s^{-1}$ (280 cfm). Therefore, for this house, approximately 60% to 85% of the pressurization fan's air flow returned to the upstairs or escaped to the attic through bypasses.

Grab samples of ^{222}Rn

Radon-222 concentrations for LBL14C are identified in Fig. 2 by the letter *R*. Samples from below basement slabs and slabs-on-grade adjacent to a below-grade basement wall usually had the highest ^{222}Rn concentrations for all test locations in or very near the houses. The average concentration for 44 of these locations was 150,000 Bq m^{-3} (with a geometric mean of 43,000 Bq m^{-3} and a GSD of 8.3) and exceeds the average concentration of 18,000 Bq m^{-3} (a GM of 6500 Bq m^{-3} and a GSD of 4.8) for 98 block wall cavities. The wall cavities are probably subjected to greater dilution by outside and house air. Radon-222 concentrations in samples from the indoor test holes at the same house often ranged from several hundred Bq m^{-3} to over 500,000 Bq m^{-3} (and in one extreme case, as high as 880,000 Bq m^{-3}).

Vacuum field extension

The pressure field developed around the substructure of LBL14C during the test with the industrial vacuum is shown in Fig. 3. (The letter *V* indicates a vacuum test ratio.) While pressure fields extended to greater distances at houses with highly permeable regions or gravel layers around the substructure, the field nonetheless dropped off very quickly with distance from the vacuum hole. An examination of data from all seven houses showed that the ΔP at 66 floor test holes correlated poorly with distance from the vacuum hole (correlation coefficient, $R = -0.23$). As observed by other workers, there are inhomogeneities and discontinuities beneath slabs that interrupt distribution of the vacuum pressure field (Gadsby et al. 1989; Fowler et al. 1989; Matthews et al. 1989). Not surprisingly, the pressure field did not extend as effectively to the test holes into and through the block walls. Other researchers have reported on results of more detailed experimental work that characterizes the application of this technique (Matthews et al. 1989; Gadsby et al. 1989).

Table 4. Comparison of measured and predicted flow rates for a basement pressurization system at LBL11.

	Measurement dates 12 Feb	21 Mar	30 Mar
Basement ΔP with pressurization fan (Pa)	3.8	4.9	5.7
Measured flow with pressurization fan on ($m^3\ s^{-1}$)	0.10	0.15	0.15
Predicted flow based on blower test of 10 Feb ($m^3\ s^{-1}$)	0.10	0.13	0.14
Predicted flow based on blower test of 20 Mar ($m^3\ s^{-1}$)	0.071	0.093	0.11

Pressure field mapping and basement depressurization

Figure 3 also displays results of pressure field mapping tests (PFM) conducted at different basement depressurizations. Data from different tests generally replicate well, having a correlation coefficient of 0.79. The mean coupling ratio for 161 indoor tests holes was 0.35, with a standard deviation (SD) of 0.29 and a median of 0.30. In particular, the average coupling ratio for 85 holes into block wall cavities was lower (0.25, with an SD of 0.25 and a median of 0.20) than that for 38 holes into the gravel below the slab (0.39, with an SD of 0.22 and a median of 0.30), or for 27 holes into soils below the gravel layer or along wall exteriors (0.48, with an SD of 0.35 and a median of 0.50). This implies that the interior of the block walls have a better coupling, through openings (e.g., mortar cracks), leakage pathways, or the porous materials of the block, to the interior of the basement than the other spaces surrounding the substructure.

Air velocities and pressure differences between the end of the test holes and the basement interior were compared for tests at different basement pressures. Velocities up to 2.5 m s^{-1} were measured in the flow adaptor during basement depressurization of 30 Pa. In general, velocities varied almost linearly with increasing ΔP. However, a number of floor and wall holes had unusually low velocities, possibly due to low-permeability materials at the ends of the holes. In two houses, pressure differences and velocities were measured at 22 test holes at several basement pressures. Velocities through test holes did not increase exactly in direct proportion to the ΔP across the test holes. A flow exponent, n, was calculated for each of the 22 test holes from

$$Q_2/Q_1 = [\Delta P_2/\Delta P_1]^n, \quad (5)$$

where Q_1, ΔP_1 = first flow and ΔP, respectively, and Q_2, ΔP_2 = second flow and ΔP, respectively.

This calculation is strictly valid only if the pressure difference across the test holes did not change appreciably when the test holes were opened to perform the flow measurements. The average value of n for these test holes was 0.92; however, the SD of 0.69 is large. The large standard deviation could result from inaccuracies in the measured velocities and pressures or from irregularities in the size and shape of the test holes and hole openings. This result suggests that errors can be expected from attempts to measure permeability through test holes into porous materials adjacent to substructures (soils, gravels, etc.), since the assumption of linear Darcy flow in those materials near the test hole may be violated.

To determine if trained technicians could use the relative flow rate of chemical smoke to accurately represent the air velocity at test holes, smoke flow data was coded and compared against measured flow velocities. Codes were from 0 (no movement observed) to 5 (very rapid movement). These codes appear to be a crude indicator of velocity that is affected by the perception of volumetric flow at holes of different size. At low velocities, the qualitative description using smoke is roughly proportional to velocity, but the technicians could not differentiate velocities larger than approximately 0.4 m s^{-1}. However, flow detection with smoke is much more sensitive than velocity and ΔP measurements and is, therefore, still a useful tool.

During 30 Pa depressurization of the basements in four houses, chemical smoke was used to detect air movement at soil grade along the exterior of substructure walls where the soil meets the wall. At every house, there was at least one location where the smoke was pulled into the gap of varying width between the house and soil. At house LBL08, smoke was also drawn into soil cracks and small depressions in the soil (approximately 0.07 m in diameter and unknown depth) near downspouts that were within 0.3 m of the substructure walls. Presumably, openings in the substructure surfaces permitted the low pressure in the basement to pull outside air into these high permeability pathways near the building.

Velocities measured at the test holes during vacuum field tests and pressure field mapping were compared in an attempt to relate the two diagnostic procedures. There was poor correspondence between the two velocities, probably due to the differences in the point(s) where the low pressure was applied.

DISCUSSION AND ANALYSIS

The visual inspection and tour of the building is an essential, if not the most important, task prior to selecting, designing, and installing a ^{222}Rn control system. This inspection can quickly direct an investigator to the important factors causing high indoor ^{222}Rn levels and the solutions that are mostly likely to reduce those levels. In buildings where diffusion of ^{222}Rn from construction materials is suspected of contributing significant ^{222}Rn into the indoor atmosphere, the relatively simple, short-term test with charcoal canisters appears to be a useful, semiquantitative measurement, although none of the houses studied here exhibited elevated indoor ^{222}Rn levels related to materials.

The alternative technique for determining ^{222}Rn-in-water concentrations by collecting grab samples of bathroom air is not recommended because of large uncertainties in measuring low ^{222}Rn concentrations (or small changes in concentration). Improvements to this technique, including more care in maintaining low backgrounds in the α-scintillation cells, longer counting of cell activity, using a more appropriate transfer coefficient, and operating the shower for a longer period, may result in more precise and accurate measurements.

By measuring the additional depressurization caused by certain appliances that operate for extended periods, solutions can be devised to eliminate or minimize this effect. According to data from these houses, attic exhaust fans can cause the greatest increase in basement depressurization; however, the longer operating times of forced-air system blowers may result in more persistent additional depressurization exacerbating the forces drawing ^{222}Rn-bearing soil gas into buildings. In addition, where these

systems have leaky return air ducts and plenums or open return air vents in the substructure, the high ^{222}Rn concentration substructure air is distributed more readily throughout the remainder of the building (Harrje et al. 1989; Revzan et al. 1987; Turk et al. 1989a).

Blower door tests were useful for comparing the air leakage of different building zones and identifying tightly sealed substructures so that basement pressurization may be considered as a control system option. Although the blower door did not accurately predict the actual flow rates measured during operation of a basement pressurization system, the predictions may be satisfactory for evaluating the feasibility of this technique. To apply the predictions correctly, the natural depressurization at the basement floor that is induced by maximum indoor-outdoor temperature differences must be estimated from the structure height and climatological data. A minimum overpressurization of 2–3 Pa is then added to the estimated natural depressurization, and the required flows are calculated at that total pressure difference. The substructure ceiling and wall/floor leakage area measurements can indicate where additional attention to sealing is necessary to reduce the flow rates required for overpressurization and reduce the energy penalty associated with the loss of conditioned air.

Soil air permeability measurements show the presence of very high-permeability regions adjacent to exterior surfaces of substructures. These regions probably consist of gravel, loosely packed backfill material, and air gaps caused by expansion/contraction cycles and settling. Since soil gas can move freely within these high-permeability regions, the natural pressure gradient at cracks or openings in substructure surfaces that connect to these regions may cause ^{222}Rn-laden soil gas to be drawn into the substructure at relatively higher rates. However, because soil gases can move freely in these high-permeability regions, the pressure fields developed by subsurface ventilation ^{222}Rn control systems may extend to greater distances around the houses, thereby reversing the natural pressure gradient at more ^{222}Rn entry locations (provided that these regions are continuous and not interrupted by impermeable barriers). Measurements of soil air permeability, along with the collection of soil samples, have furnished useful research information but are not essential for the private contractor.

Soil gas and ^{222}Rn *entry potentials*

While none of the procedures associated with the pressure field mapping and vacuum field extension tests can provide foolproof guidance for the design of SSV mitigation systems and a guarantee of the eventual long-term effectiveness of these systems, some of the data from the field measurements may be used to develop parameters that quantify (approximately) the potential for soil gas and ^{222}Rn to enter a building at different locations. The low coupling ratios indicate regions surrounding substructures that, in some way, have good connection to the interior of the substructure. By itself, good coupling of the pressure field to a test hole location does not confirm that large quantities of soil gas enter the building through nearby openings.

The soil, aggregate, or backfill material around the substructure must also be sufficiently permeable so that substantial soil gas can be transported to the openings. Therefore, a location near the substructure with good pressure coupling to the interior of the substructure and with a relatively high flow through a test hole is a likely entry location for significant quantities of soil gas. There are many such regions near houses as indicated by high values of permeability, high air velocities measured at test holes during pressure field mapping tests, and by the observation of air movement along the below-grade surfaces of exterior walls caused by the ΔP in the substructure.

The passage of soil gas into a substructure depends upon the flow path resistances through the materials surrounding the substructure and through the surfaces of the substructure. A simplified electrical analog of the house-soil system can be created to simulate the flows, pressure drops, and resistances in the soils, near-house materials, and substructure surfaces (Fig. 4). Two measurement conditions are shown: the test hole sealed and the test hole open (indicated by dotted lines representing the flow, $Q_H(I_H)$, and resistance, R_H, of the test hole and flow adaptor). Following are definitions where the corresponding electrical analogs are indicated in parentheses (use of the subscript C with any of these terms identifies the condition with the test hole closed):

$Q_H\,(I_H)$ = measured (corrected) flow through open test hole and flow adaptor ($m^3\ s^{-1}$);
$Q_F\,(I_F)$ = (defined) flow through cracks and openings in below-grade substructure surfaces with test hole open ($m^3\ s^{-1}$);
$Q_T\,(I_T)$ = (defined) total flow through cracks, openings, and open test hole ($m^3\ s^{-1}$);
$P_B\,(V_B)$ = measured pressure difference between inside of basement and outside, point a to c (Pa);
$P_H\,(V_H)$ = calculated pressure drop across open test hole and flow adaptor, point a to b (Pa);
$P_S\,(V_S)$ = pressure drop across soil paths between point b and outside with test hole open ($=P_B - P_H$) (Pa);
R_H = (defined) resistance of open test hole and flow adaptor (Pa-s m^{-3});
$R_{F\text{-}EFF}$ = calculated effective resistance that lumps resistances of cracks and openings in substructure surfaces and resistances of near-surface materials surrounding the open test hole (R_{F1}, R_{F2}, R_{F3}, etc.) (Pa-s m^{-3}); and
$R_{S\text{-}EFF}$ = calculated effective resistance of soil paths to measurement point b (R_{S1}, R_{S2}, R_{S3}, etc.), with test hole open (Pa-s m^3).

No velocity corrections were made based on test hole size or configuration. These corrections are estimated to have been less than ±10%. Drilling all holes to the same diameter is the preferred alternative. To compute the vol-

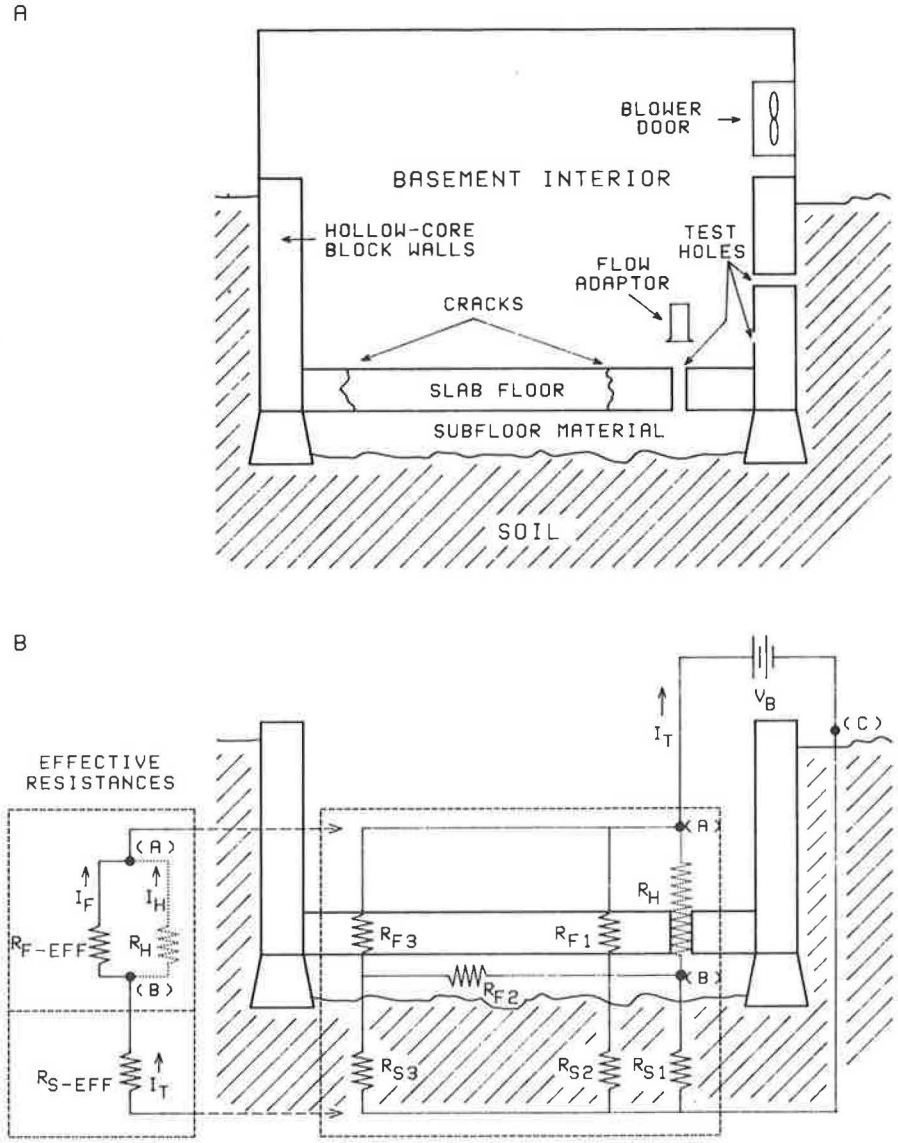

Fig. 4. Drawing of substructure during pressure field mapping and basement depressurization (A). A simplified electrical analog of the various flows, pressure drops, and resistances during the test depicted in (A) is shown in (B). The dotted line indicates the variables associated with an open test hole. A further simplification is shown by the circuit on the left side of (B).

umetric flow rates, we used the measured velocities and the cross-sectional area of the flow adaptor minus the projected area of the hot wire anemometer probe. For pressure differences and flow rates that were below detection limits, values of 0.5 times the detection limit were assumed. Final results are insensitive to this assumption.

Pressure drops across the flow adaptor and test hole (P_H) were estimated using the engineering formula for laminar flow through a tube:

$$-\frac{P_H}{x} = \frac{8\mu Q_H}{\pi r^4}, \qquad (6)$$

where x = length of test hole plus flow adaptor (m), μ = absolute viscosity of air, 1.8×10^{-5} kg m^{-1} s^{-1}, and r = radius of the tube. (In our case, we used the radius of the flow adaptor of 0.0045 m.) Estimated pressure drops ranged from less than 0.01 Pa to 3.5 Pa. In theory, a more accurate value for this pressure drop could be determined by direct measurement; however, the small pressure differences are difficult to measure in practice.

We assume that the complex network of resistances through the soil and substructure surfaces can be represented approximately by the simplified circuit shown to the left in Fig. 4b. With the test hole sealed, a resistance ratio (Z), i.e., the resistance of the substructure surfaces and near-surface materials divided by the resistance of the soil, can be defined as:

$$Z = \frac{V_{HC}}{V_{SC}} = \frac{I_{TC}R_{FC\text{-}EFF}}{I_{TC}R_{SC\text{-}EFF}} = \frac{R_{FC\text{-}EFF}}{R_{SC\text{-}EFF}}; \text{ thus} \quad (7)$$

$$R_{FC\text{-}EFF} = Z(R_{SC\text{-}EFF}). \quad (8)$$

Using Kirchoff's rules for circuit analysis when the test hole is open, the following three independent equations are derived:

$$V_B - I_H R_H - I_T R_{S\text{-}EFF} = 0, \quad (9)$$

$$I_F R_{F\text{-}EFF} - I_H R_H = 0, \text{ and} \quad (10)$$

$$I_T - I_F - I_H = 0. \quad (11)$$

If we assume that $R_{FC\text{-}EFF} \sim R_{F\text{-}EFF}$ and $R_{SC\text{-}EFF} \sim R_{S\text{-}EFF}$, then we can solve for $R_{S\text{-}EFF}$, using eqn (8) through (11) and substituting for analogous parameters to obtain:

$$R_{S\text{-}EFF} = \frac{P_B - P_H(1 + Z^{-1})}{Q_H}. \quad (12)$$

$R_{F\text{-}EFF}$ can be determined from eqn (8).

Detailed flows and pressure measurements were made at four of the seven houses, with the basements depressurized to approximately −10 Pa using the blower door. The calculated effective resistances for 117 test holes (including some replicates) at the four houses are summarized in Table 5. The data are highly variable, as indicated by the large standard deviations. However, by examining the geometric means, several patterns are apparent and statistically significant: (1) the effective soil resistance that is "seen" by test locations across the slab floors and in block cavities is similar, probably because large surface areas of soil (and for the block walls, areas exposed directly to the outside air) are accessible to these holes; (2) the slab floors are approximately five times more resistant to soil gas movement than the interior surface of the porous block walls; and (3) for all locations, except those in the soil exterior to the walls, the substructure "sees" the soil as being a factor of 2 to 7 more resistant to soil gas flow than the substructure surfaces and materials very near to the substructure.

We also find that the entire thickness of a block wall is many times more resistant to soil gas flow than only the interior surface of the block, presumably because of the coatings and sealants that are applied to the exterior surface for waterproofing. These data support the view that the flow of soil gas into buildings depends to a lesser degree on the resistance of the building surfaces below grade than on the resistance of the surrounding soil and materials. It is important to recognize that low resistance values can result from low resistance in the materials near to the test locations or from the sum of many parallel resistances when the test location "sees" a large area of soil and building material.

We can define the entry potential (net conductance) for soil gas, G ($m^3\ Pa^{-1}\ s^{-1}$), from:

$$I_T = \frac{V_B}{R_{S\text{-}EFF} + R_{F\text{-}EFF}}, \quad (13)$$

or

$$G = \frac{1}{R_{S\text{-}EFF} + R_{F\text{-}EFF}} \propto Q_T. \quad (14)$$

Values of G ranged from less than 0.01×10^{-6} $m^3\ Pa^{-1}\ s^{-1}$ to 3.2×10^{-6} $m^3\ Pa^{-1}\ s^{-1}$. The data for LBL14C are plotted in Fig. 3. This figure and data from the four houses in Table 6 show that the soil gas entry potentials for the

Table 5. Statistical summary of effective resistances for soils and substructure surfaces from four houses.

	Test hole location			
	Below slab gravel	Block wall cavity	Exterior to wall	All locations
Soils, $R_{S\text{-}EFF}$ (10^6 Pa-s m^{-3})				
Geometric mean	1.1	0.78	2.6	1.0
Geometric std. dev.	5.1	2.5	5.4	3.7
Median	0.58	0.71	1.6	0.73
Arithmetic mean	5.7	1.6	8.5	3.6
Arithmetic std. dev.	13	3.8	14	9.4
Number	33	69	15	117
Substructure surfaces, $R_{F\text{-}EFF}$ (10^6 Pa-s m^{-3})				
Geometric mean	0.55	0.11	4.6	0.28
Geometric std. dev.	5.1	2.5	7.9	6.3
Median	0.43	0.11	4.7	0.18
Arithmetic mean	2.7	0.16	18	3.1
Arithmetic std. dev.	6.8	0.19	29	12
Number	33	69	15	117

Table 6. Statistical summary of soil gas and Rn entry potentials from four houses.

	Test hole location			
	Below slab gravel	Block wall cavity	Exterior to wall	All locations
Soil gas entry potential, G (10^{-6} m^3 Pa^{-1} s^{-1})				
Geometric mean	0.5	1.2	0.11	0.73
Geometric std. dev.	4.8	1.6	4.3	3.6
Median	1.2	1.3	0.17	1.2
Arithmetic mean	1.1	1.4	0.24	1.1
Arithmetic std. dev.	0.85	0.52	0.28	0.70
Number	22	44	9	75
Radon-222 entry potential, E (10^{-3} Bq Pa^{-1} s^{-1})				
Geometric mean	23	7.9	3.2	9.7
Geometric std. dev.	6.7	5.1	6.4	6.2
Median	31	8.1	3.4	11
Arithmetic mean	110	24	21	48
Arithmetic std. dev.	280	42	54	160
Number	22	42	9	73

hollow-core block walls are higher than for the other locations, probably because of the lower effective resistance of the block material and the large exterior surface area of wall exposed to soil and/or outdoor air. Note that the area over which the effective resistances and entry potential are applied is not defined.

The soil gas entry potential at a particular location is affected by all soils, materials, and openings in the surfaces around a building, but more so by those nearby or connected by a high-permeability path. In an ideal situation, where the subfloor materials are highly permeable (R_{F2} is small) and the substructure surfaces and surrounding soils are homogeneous—without dicontinuities such as impermeable barriers or large short circuits—a single test hole location would suffice to calculate the total resistance of the substructure surfaces and of the soils. However, many of these discontinuities may exist around typical houses. Consequently, more than one measurement location is required to determine the local resistances at different locations. Unfortunately, in this situation with many test locations, it is difficult to know the distance from each test location over which the resistances are derived. Indeed, for those test locations in homogeneous materials such as subfloor gravel layers, identical conditions may be measured over a large area. While at the same house, measurements made at test locations in different materials could represent conditions very near to the test location. More study is required to determine the distance from a test hole over which the soil gas entry potential is applicable. When this relationship is better understood, the test holes can be better placed to best represent the soil gas entry throughout the entire substructure.

To describe the potential for ^{222}Rn entry into a building at a location, another parameter is necessary. This number, the ^{222}Rn entry potential, E(Bq Pa^{-1} s^{-1}), can be defined by multiplying the soil gas entry potential by the ^{222}Rn concentration, C(Bq m^{-3}), in a grab sample of air collected from the test hole:

$$E = GC. \tag{15}$$

Thus, the ^{222}Rn entry potential should indicate the likelihood that significant amounts of ^{222}Rn can enter a substructure at a particular location. In this study, grab samples were not always collected from the test holes concurrently with the measurements of flow and pressure drop. Therefore, ^{222}Rn concentrations from grab samples collected at other times were averaged and used to compute the ^{222}Rn entry potential. The data are summarized in Fig. 3 and Table 6.

For a similar set of 73 holes in four houses, the geometric mean ^{222}Rn entry potential was, on average, highest for the test holes into the subslab aggregate. Although the block wall test holes had a slightly higher soil gas entry potential, the subslab test holes had greater concentrations of ^{222}Rn in the soil gas that compensated for their smaller soil gas entry potential. Calculated values of E ranged from less than 0.1×10^{-3} Bq Pa^{-1} s^{-1} to 1300×10^{-3} Bq Pa^{-1} s^{-1}.

When ^{222}Rn entry potential data are plotted on plans of all four houses, similar to Fig. 3, we find that the areas of highest ^{222}Rn entry potential generally coincide with the locations where pipes of successful SSD systems were placed through the slabs. For these houses, a "high" ^{222}Rn entry potential would be considered greater than approximately 15×10^{-3} Bq Pa^{-1} s^{-1}. Since the entry potentials were calculated after installation of the SSD systems, these indices appear to provide a quantitative method for replicating the intuitive approach of successful mitigation contractors. LBL12 is an exception, where it was difficult

to bring indoor ^{222}Rn levels below the target of 148 Bq m^{-3}. A review of the data from this house indicates areas of high ^{222}Rn entry potential that were not in proximity to an SSD pipe and may have been the sources of inadequately controlled Rn entry.

In general, the ^{222}Rn entry potential indicates the preferred locations for SSD pipes but does not provide information about the ability of a specific SSV system to reduce ^{222}Rn entry rates. The vacuum field extension test remains the best technique to measure the extent to which a SSD system can reverse the natural pressure gradient around a substructure and therefore control ^{222}Rn entry. Therefore, combining the vacuum test with identified areas of high ^{222}Rn entry potentials can benefit decisions for placement of SSV pipes. When the soil gas entry potential is high but communication or connection to the vacuum location is poor for a particular test point, obstructions or high-permeability short circuits are probably blocking or intercepting the extension of the pressure field from the vacuum. The problem is then to provide access to the areas of high ^{222}Rn entry potential.

The geometric mean of the ^{222}Rn entry potentials for each of the four houses was compared with the average indoor ^{222}Rn concentration, measured between 1 September and 1 May and weighted by the volumes for various zones where indoor ^{222}Rn was measured. From the lowest to highest average indoor ^{222}Rn concentration, 540, 620, 650, and 660 Bq m^{-3}, the geometric mean ^{222}Rn entry potentials were 6.4, 10, 7.2, and 18×10^{-3} Bq Pa^{-1} s^{-1}, respectively. For the third house listed (LBL13), the GM ^{222}Rn entry potential fails to trend with increasing indoor ^{222}Rn concentrations and suggests weaknesses in the current development or application of the new parameters.

The time-varying nature of many of the measured parameters makes comparisons with indoor ^{222}Rn levels difficult. Although ^{222}Rn concentrations in diagnostic grab samples collected from the test holes in the substructure under mechanically induced depressurization are, on average, representative of concentrations measured under natural conditions, the ^{222}Rn concentrations under natural conditions showed large variations during the study. It would not be surprising to also observe changes in the soil gas entry potential due to changes in soil permeability (caused by precipitation). Therefore, a one-time determination of soil gas and ^{222}Rn entry potentials may not be representative of entry potentials typical for a house. More study on the variability of near-house ^{222}Rn concentrations and soil permeability is required.

In addition, the assumptions, $R_{FC\text{-}EFF} = R_{F\text{-}EFF}$ and $R_{SC\text{-}EFF} = R_{S\text{-}EFF}$, are only approximations, since the paths for air flowing through the soil and building surfaces are different in the two measurement conditions. The effects of inhomogeneities in soils, in materials near the house, and in substructure surface materials on the assumption have not been examined. Although the derivation of eqn (12) is generally not sensitive to the pressure drop across the test hole and flow adaptor, the right term in the numerator of that equation was occasionally as large as 55% of the substructure depressurization (P_B). This term has the greatest impact when the pressure drop across the test hole is large or when substructure surfaces are leaky (small Z). Although a larger substructure-outside pressure difference (P_B) developed by the blower door does not simulate actual house operating conditions, it does increase the magnitude of most parameters so that they can be more easily measured. By artificially depressurizing the building, many seasonal effects can be minimized and another short-term test that is being evaluated can be conducted simultaneously to simulate winter indoor ^{222}Rn concentrations.

CONCLUSION

Two new parameters that describe the potential for soil gas and ^{222}Rn to enter through substructure surfaces have been defined. They are based on relatively easily performed measurements of ^{222}Rn concentrations near substructure surfaces and flows and pressures across those surfaces. These parameters are imperfect but useful (1) to identify areas in a substructure with the potential for comparatively high soil gas entry rates; (2) to compare the relative leakiness of below-grade surfaces in different houses; (3) to provide approximate measures of the resistance of substructure surfaces and soils/materials around the substructure; and (4) to identify areas in a substructure with potentially high ^{222}Rn entry rates for placement of Rn control systems. Determination of these parameters in additional houses and under changing seasonal conditions is necessary to more fully examine their suitability as diagnostic and research tools.

Acknowledgments—The authors would like to thank the families of the seven homes in New Jersey for their patience and hospitality; coworkers Jacques Hill, Barbara Moed, Tim Nuzum, and Al Smith for their assistance in conducting measurements and analyzing samples; Mark Modera for thought-provoking discussions; Michael Apte, William Fisk, and Ashok Gadgil for their reviews; Mary Cahill of the New Jersey Department of Environmental Protection for on-site logistical support in New Jersey; Ted Gartner and Leslie Turk for document preparation; and David Sanchez of the AEERL, U.S. EPA for program support and oversight. This work was supported by the Assistant Secretary for Conservation and Renewable Energy, Office of Building and Community Systems, Buildings Systems Division, by the Director, Office of Energy Research, Office of Health and Environmental Research, Human Health and Assessments Division and Pollutant Characterization and Safety Research Division of the U.S. Department of Energy (DOE) under contract No. DE-AC03-76SF00098, and by the U.S. Environmental Protection Agency (EPA) through Interagency Agreement DW89931876-01-0 with DOE. Although the research described here is partially supported by the U.S. EPA, this report has not been subjected to EPA review. Its contents do not necessarily reflect the views and policies of the EPA, nor does mention of firms, trade names, or commercial products constitute endorsement or recommendation for use.

REFERENCES

American Society for Testing and Materials. Standard practice for measuring air leakage by the fan-pressurization method. Philadelphia: ASTM: ASTM E 779–81; 1981.

Brennan, T. M. Reducing indoor radon: A training manual. (2nd ed.). Albany, NY: New York State Energy Office; 1988.

DSMA Atcon Ltd. Review of existing instrumentation and eval-

uation of possibilities for research and development of instrumentation to determine future levels of radon at a proposed building site. Ottawa, Canada: Atomic Energy Control Board; Report INFO-0096; 1983.

Fowler, C. S.; Williamson, A. D.; Pyle, B. E.; Belzer, F. E.; Sanchez, D. C.; Brennan, T. M. Sub-slab depressurization demonstration in Polk County, Florida, slab-on-grade houses. In: Proceedings of 1988 Symposium on Radon and Radon Reduction Technology. Research Triangle Park, NC: U.S. EPA; EPA-600/9-89/006a, Vol 1; 1989:7-65 to 7-78.

Gadsby, K. J.; Hubbard, L. M.; Harrje, D. T.; Sanchez, D. C. Rapid diagnostics: Subslab and wall depressurization systems for control of radon. In: Proceedings of 1988 Symposium on Radon and Radon Reduction Technology. Research Triangle Park, NC: U.S. EPA; EPA-600/9-89/006a, Vol 1; 1989:3-69 to 3-85.

Gesell, T. F.; Prichard, H. M. The contribution of radon in tap water to indoor radon concentrations. In: Proceedings of the Symposium on the Natural Radiation Environment III. Springfield, VA: NTIS; U.S. Department of Energy; CONF-80422; 1980:1347–1363.

Harrje, D. T.; Hubbard, L. M.; Gasdby, K. J.; Bolker, B.; Bohac, D. L. The effect of radon mitigation systems on ventilation in buildings. ASHRAE Transactions 95, part 1:107–113; 1989.

Harrje, D. T.; Hubbard, L. M.; Sanchez, D. C. Proceedings of the Radon Diagnostics Workshop. Princeton: Princeton University; CEES Report No. 223; 1987.

Matthews, T. G.; Wilson, D. L.; TerKonda, P. K.; Saultz, R. J.; Goolsby, G.; Burns, S. E.; Haas, J. W. Radon diagnostics: Subslab communication and permeability measurements. In: Proceedings of the 1988 Symposium on Radon and Radon Reduction Technology. Research Triangle Park, NC: U.S. EPA-600/9-89/006a, Vol 1; 1989:6-45 to 6-66.

Mowris, J. J.; Fisk, W. J. Modeling the effects of exhaust ventilation on radon entry rates and indoor radon concentrations. Health Phys. 54:491–501; 1987.

Nazaroff, W. W.; Doyle, S. M.; Nero, A. V.; Sextro, R. G. Potable water as a source of airborne radon-222 in U.S. dwellings: A review and assessment. Health Phys. 52:281–295; 1985.

Nazaroff, W. W.; Lewis, S. R.; Doyle, S. M.; Moed, B. A.; Nero, A. V. Experiments on pollutant transport from soil into residential buildings by pressure-driven air flow. Environ. Sci. Technol. 21:459–466; 1986.

Nero, A. V.; Nazaroff, W. W. Characterizing the source of radon indoors. Radiat. Prot. Dosim. 7:23–29; 1984.

Revzan, K. L.; Turk, B. H.; Harrison, J.; Nero, A. V.; Sextro, R. G. Parametric modeling of temporal variations in radon concentrations in homes. IEEE Transactions on Nucl. Sci. 35(1):550–555; 1987.

Sanchez, D. C.; Hubbard, L. M.; Harrje, D. T.; Turk, B. H. The use of diagnostic measurements to enhance the selection and effectiveness of radon mitigation for detached dwellings. In: Seifert, B.; Esdorn, H.; Fischer, M.; Ruden, H.; Wegner, I., eds. Indoor air '87: Proceedings of the Fourth International Conference on Indoor Air Quality and Climate. Berlin: Institute for Water, Soil and Air Hygiene; 1987(2):370–375.

Sextro, R. G.; Nazaroff, W. W.; Turk, B. H. Spatial and temporal variations in factors governing the radon source potential of soil. In: Proceedings of the 1988 Symposium on Radon and Radon Reduction Technology. Research Triangle Park, NC: U.S. EPA; EPA-600/9-89/006a, Vol. 1; 1989:5-61 to 5-74.

Turk, B. H.; Harrison, J.; Prill, R. J.; Sextro, R. G. Interim report on diagnostic procedures for radon control. Berkeley, CA: Lawrence Berkeley Laboratory; Report No. LBL-23089; 1987a.

Turk, B. H.; Harrison, J.; Prill, R. J.; Sextro, R. G. Intensive radon mitigation research. Lessons learned. In: Proceedings of the Symposium on Radon and Radon Reduction Technology. Research Triangle Park, NC: U.S. EPA; EPA-600/9-89/006a, Vol 1; 1989a:6-25 to 6-44.

Turk, B. H.; Harrison, J.; Prill, R. J.; Sextro, R. G. Developing soil gas and radon entry potentials for substructure surface and assessing radon control diagnostic techniques. Berkeley, CA: Lawrence Berkeley Laboratory; Report No. LBL-27319 Rev., with appendices; 1989b.

Turk, B. H.; Harrison, J.; Sextro, R. G.; Hubbard, L. M.; Gadsby, K. J.; Matthews, T. G.; Dudney, C. S.; Sanchez, D. C. Evaluation of radon reduction techniques in fourteen basement houses: Preliminary results. In: Proceedings of the 81st Annual Meeting of the Air Pollution Control Association, Dallas, TX; Pittsburgh, PA: APCA; Paper 88-107.2; 1988.

Turk, B. H.; Prill, R. J.; Fisk, W. J.; Grimsrud, D. T.; Moed, B. A.; Sextro, R. G. Radon and remedial action in Spokane River Valley homes. Volume 1: Experimental design and data analysis. Berkeley, CA: Lawrence Berkeley Laboratory; Report No. LBL-23430; 1987b.